ELSEVIER

Polymer 43 (2002) 3335–3343

polymer

www.elsevier.com/locate/polymer

Crystallization kinetics and morphology of poly(trimethylene terephthalate)

Po-Da Hong*, Wei-Tsung Chung, Ching-Fu Hsu

Department of Fiber and Polymer Engineering, National Taiwan University of Science and Technology, Taipei 10607, Taiwan, ROC

Received 14 September 2001; received in revised form 11 January 2002; accepted 21 February 2002

Abstract

In this work, the isothermal crystallization kinetics of polytrimethylene terephthalate (PTT) was first investigated from two temperature limits of melt and glass states. For the isothermal melt crystallization, the values of Avrami exponent varied between 2 and 3 with changing crystallization temperature, indicating the mixed growth and nucleation mechanisms. Meanwhile, the cold crystallization with an Avrami exponent of 5 indicated a character of three-dimensional solid sheaf growth with athermal nucleation. Through the analysis of secondary nucleation theory, the classical regime I → II and regime II → III transitions occurred at the temperatures of 488 and 468 K, respectively. The average work of chain folding for nucleation was ca. 6.5 kcal mol^{-1}, and the maximum crystallization rate was found to be located at ca. 415 K. The crystallite morphologies of PTT from melt and cold crystallization exhibited typical negative spherulite and sheaf-like crystallite, respectively. Moreover, the regime I → II → III transition was accompanied by a morphological transition from axialite-like or elliptical-shaped structure to banded spherulite and then non-banded spherulite, indicating that the formation of banded spherulite is very sensitive to regime behavior of nucleation.

Keywords: Poly(trimethylene terephthalate); Crystallization; Banded spherulite

1. Introduction

Polytrimethylene terephthalate (PTT) is a promising material for engineering plastic and textile fiber, and in particular it combines many advantages of nylons and other polyesters [1–3]. PTT has also been introduced as a commercial polymer, joining the polyester family like polyethylene terephthalate (PET) and polybutylene terephthalate (PBT). Ward and Wilding [4] found that PTT exhibits better elastic recovery than PET and PBT. Owing to higher elastic recovery, PTT has been widely studied recently [5–9].

The study of bulk crystallization kinetics of polymers is an important step in understanding, predicting, and designing structural formation under various processing conditions. In general, the well-known Avrami equation and secondary nucleation theory could describe well the crystallization kinetics of polymers. Recently, Huang and Chang [9] have studied the crystallization behavior for PTT from melt state and compared some crystallization parameters with those reported in the literatures for PET and PBT. They reported that the work of chain folding for nucleation in PTT was ca. 4.8 kcal mol^{-1}, which is much lower than that of PET (ca. 10 kcal mol^{-1}) [10] but very close to that of PBT (ca. 5 kcal mol^{-1}) [11]. Due to different chain structures with various number of methylene groups among these polyesters, the chain flexibility of PTT should be higher than that of PET but lower than that of PBT. This fact must reflect the difference in the work of chain folding between PTT and PBT. Therefore, the value of the work of chain folding for PTT reported by Huang and Chang may be necessary to be reconsidered, if the chain folding for nucleation is really related to the chain stiffness.

Generally, the complete relationship between crystallization temperature and crystallization rate is difficultly obtained when the crystallization rate is too fast. In fact, only few polymers such as PEEK [12], PPS [13] and PET [14] could get a complete relationship of temperature-dependent crystallization rate between T_g and T_m. Owing to fast crystallization for PTT compared with that for PET, the crystallization from glass state for PTT has not been reported so far. In this work, we paid attention to the analysis of the isothermal melt and cold crystallization behaviors for PTT. In addition, the secondary nucleation analysis [15] was used as well to compare the work of chain folding among these well-known aromatic polyesters such as PET and PBT. Finally, the morphological changes

* Corresponding author. Tel.: +886-2-27376539; fax: +886-2-27376544.

E-mail address: phong@tx.ntust.edu.tw (P.-D. Hong).

0032-3861/02/$ - see front matter
PII: S0032-3861(02)00163-5

of spherulites at various crystallization conditions are investigated using polarized light microscopy (PLM) and atomic force microscopy (AFM) observations. The banded extinction was found in PTT spherulite from melt crystallization in this work. The formation of banded spherulite was considered to be attributed to lamellar twisting along the direction of radial growth [16–19]. It is generally realized that the surface stress induced by the deep quenching of melt sample would make the lamellae twist during crystallization. In the present study, we found that the formation of banded spherulite in PTT may be concerned with the regime behavior of nucleation. The crystallization behavior accompanied by a morphological change of PTT spherulite is elucidated in this work.

2. Experimental

2.1. Materials

Polytrimethylene terephthalate (PTT) was supplied by Industrial Technology Research Institute (ITRI), Taiwan. The PTT used in this work is obtained by the direct esterification of 1,3-propanediol (PDO) with terephthalic acid (TPA) in the melt phase with tetraisopropyl titanate as the catalyst. The intrinsic viscosity of the PTT obtained from a phenol/tetrachloroethane (60/40) mixed solution at 298 K is ca. 0.84 ml/g. According to the result reported by Chuah et al. [20], the relationship between the number-average molecular weight and intrinsic viscosity of the PTT is $[\eta]_{\text{phenol/tetrachloroethane}} = 5.36M_{\text{n}}^{0.69}$. Therefore, the M_{n} of the PTT used can be estimated as ca. 43 000. All specimens were dried at 363 K for 6 h under vacuum before any new thermal treatments or experimental characterizations.

2.2. Measurements

Differential scanning calorimetry (DSC) measurements were carried out using a Perkin–Elmer Pyris 1 equipment. The isothermal melt crystallization was made by melting the sample at 553 K for 5 min and then the sample was quickly cooled at 200 K/min to an ambient crystallization temperature. For the isothermal cold crystallization, the sample was first melted at 553 K and then rapidly cooled to low temperature with liquid nitrogen for obtaining a wholly amorphous specimen. Fig. 1 shows the DSC and X-ray results of the amorphous sample. The DSC result showed that the total exothermic enthalpy is almost the same as the melting enthalpy. On the other hand, the X-ray profile exhibited only an amorphous scattering pattern without any crystalline diffraction. Then this wholly amorphous sample was heated at 200 K/min to an ambient crystallization temperature for cold crystallization. All DSC measurements were performed under a dry nitrogen atmosphere. The instrument was calibrated in both the temperature and melting enthalpy with standard samples of indium and zinc. To avoid an uneven thermal conduction through the samples, which may cause different amounts of broadening and shifting of the peak position, the aluminum pan was always filled with the same quantity of 10 ± 1 mg.

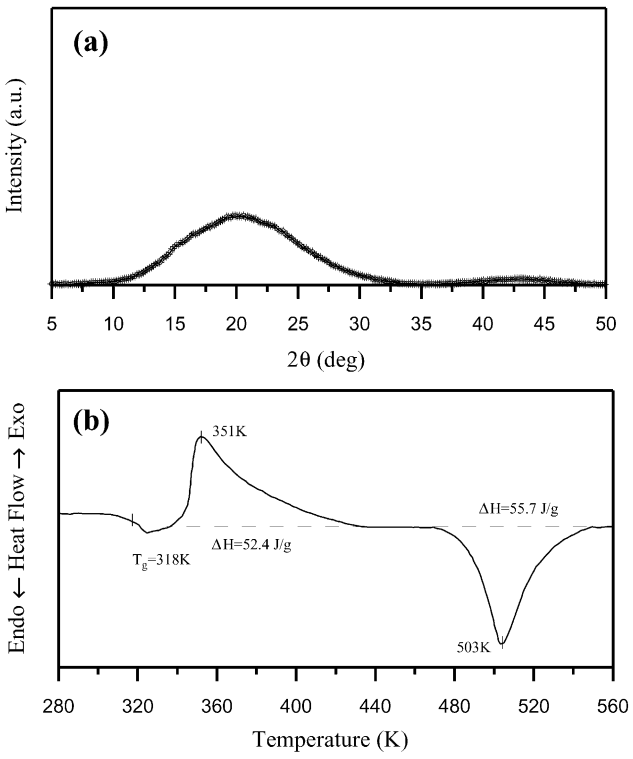

Fig. 1. (a) X-ray and (b) DSC results for wholly amorphous PTT.

The radial growth of PTT spherulite was observed using a polarized light microscopy (Leica Laborlux 12 Pols) with a hot stage (Linkam CI93). The sample was first melted at 553 K for 5 min and then rapidly cooled to the selected crystallization temperature. When the crystallization temperature was reached, the radial growth of the spherulite was recorded with a CCD camera taken as a function of time, up to the impingement of spherulites.

The surface morphology was observed using atomic force microscopy (AFM). Tapping mode AFM was used to obtain height and phase imaging data simultaneously on the Nano-Scope III setup (Digital Instruments). The 14.7 μm scanner was selected and the data were collected in 512 × 512 pixels per image.

3. Results and discussion

3.1. Avrami theory analysis

Generally, the crystallization kinetics of polymers is analyzed using a classical Avrami equation [21–23] as given in Eq. (1)

$$1 - X_t = \exp(-kt^n) \tag{1}$$

where X_t is the development of crystallinity X_{c} at time t. The

fraction of X_t is obtained from the area of the exothermic peak in DSC isothermal crystallization analysis at a crystallization time t divided by the total area under the exothermic peak

$$X_t = \frac{\int_0^t (\mathrm{d}H/\mathrm{d}t)\mathrm{d}t}{\int_0^\infty (\mathrm{d}H/\mathrm{d}t)\mathrm{d}t},$$

where the numerator is the heat generated at time t and the denominator is the total heat generated up to the complete crystallization. In Eq. (1), the k value is the Avrami rate constant and the n value is the Avrami exponent. Both k and n depend on the nucleation and growth mechanisms of spherulites. In order to deal conveniently with the operation, Eq. (1) is usually rewritten as the double logarithmic form as follows:

$$\ln\{-\ln[1 - X_t]\} = \ln k + n \ln t \quad (2)$$

The k and n values could be directly obtained using Eq. (2) from the slope and intercept of the best-fit lines, as shown in Fig. 2. It is usual to distinguish the crystallization behavior at the linear stage, i.e. before the kinetic curve deviates markedly from the theoretical isotherms as well as the primary crystallization and the secondary crystallization occur at the non-linear stage. The primary crystallization consists of the outward growth of lamellar stacks until impingement and the secondary crystallization, which may well overlap the primary crystallization, is filling in the spherulites of interstices. Many results have been suggested that both primary and secondary crystallizations were incorporated into Avrami theory [24,25]. In the present work, we focus only on primary crystallization. Some kinetic parameters for melt and cold crystallizations at various T_cs for PTT are listed in Table 1.

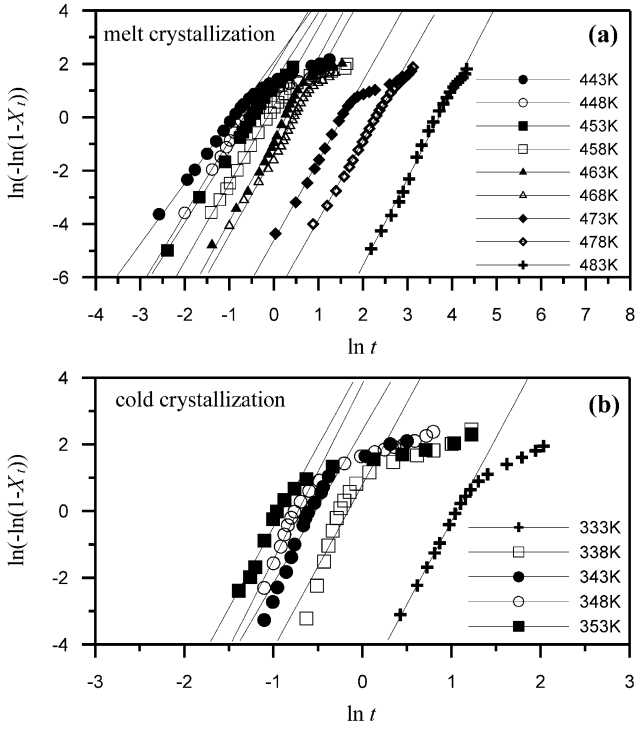

Fig. 2. Plots of $\ln(-\ln(1 - X_t))$ versus $\ln t$ for PTT (a) melt crystallization; (b) cold crystallization.

From Table 1, the n values of melt crystallization are non-integral in the range between 2 and 3. Similar result in PTT has been reported by Chuah [26]. Generally, the n value close to 3 indicates an athermal nucleation process followed by a three-dimensional crystal growth. On the other hand, the n value close to 2 may hint an athermal nucleation process followed by a two-dimensional crystal growth [27]. Our results indicate that the nucleation mechanism depends much on crystallization temperature. The non-integral n value may also be considered due to the crystal branching and/or two-stage crystal growth and/or mixed growth and nucleation mechanisms [27,28]. Regarding the cold crystallization in PTT, the average value of $n = 5$ indicates a solid sheaf growth with athermal nucleation. This crystallization type can be realized experimentally by cold crystallization [27,29]. When the crystallization temperature was close to T_g, the mobility of polymer chain dominates mainly the crystallization rate. As for cold crystallization, the diffusion of polymer segments becomes very difficult. Only the nearest neighbors of polymer segments could associate with each other for intermolecular crystallization, resulting in a sheaf-like crystallite. The k value decreases and increases, respectively, for melt and cold crystallization with increasing T_c, indicating various characteristics of the crystallization rate at the proximity of T_m and T_g. The temperature dependence of the k value is discussed in detail in Section 3.3.

3.2. Analyses from secondary nucleation theory

Linear increase in spherulite radius with time was observed at various T_cs for PTT. The rate of spherulite growth G as a function of T_c is shown in Fig. 3. A general expression has been extensively used in the analysis of

Table 1
Values for the Avrami parameters, k and n for crystallized PTT obtained from Eq. (1)

Melt crystallization			Cold crystallization		
T_c (K)	k (min^{-n})	n	T_c (K)	k (min^{-n})	n
443	7.9	2.3	328	5.01×10^{-3}	5.0
448	6.41	2.7	333	2.18	4.9
453	3.67	2.6	338	12.56	4.9
458	1.53	2.9	343	45.03	5.2
463	0.43	3.0	348	79.93	4.9
468	0.24	3.0	–	–	–
473	9.96×10^{-3}	2.9	–	–	–
478	1.1×10^{-3}	2.9	–	–	–
483	5.75×10^{-6}	3.2	–	–	–

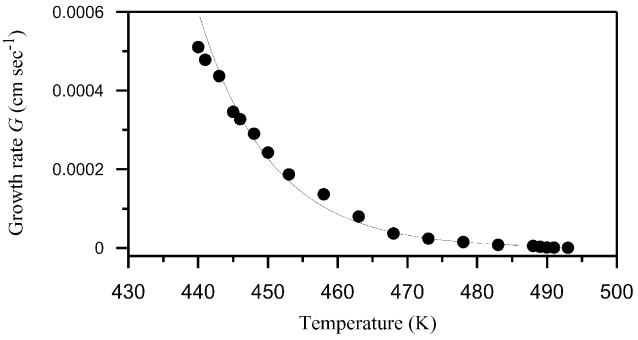

Fig. 3. Plot of linear growth rate of PTT spherulite as a function of T_c.

linear growth rate by the Hoffman–Lauritzen equation [15]

$$G = G_0 \exp\left[\frac{-U^*}{R(T_c - T_\infty)}\right]\exp\left[\frac{-K_g}{T_c(\Delta T)f}\right] \quad (3)$$

where G_0 is a pre-exponential factor independent of temperature. The first exponential term in Eq. (3) contains the contribution of diffusion process to the growth rate, where U^* is the activation energy of the molecular transferring through the melt–crystal interface, T_∞ is the temperature below such diffusion stops and R is the gas constant. The second exponential term is the contribution of nucleation process, where K_g is the activation energy of nucleation for a crystal with a critical size and strongly depends on the degree of undercooling (i.e. $\Delta T = T_m^0 - T_c$). The f factor is a correction coefficient for the temperature dependence of enthalpy of fusion, which is close to unity at high temperature (i.e. $f = 2T_c/(T_m^0 + T_c)$). In order to obtain a best fit for the secondary nucleation theory, two parameters should be predefined from our previous study [30] for PTT, i.e. the equilibrium melting enthalpy $\Delta H_f^0 = 28.8$ kJ mol^{-1} and the equilibrium melting temperature, $T_m^0 = 525$ K.

From general thermodynamic consideration, the factor K_g is very important because it contains the variable n_e reflecting the regime behavior. K_g is given by

$$K_g = \frac{n_e b_0 \sigma \sigma_e T_m^0}{\Delta H_f^0 \kappa} \quad (4)$$

where n_e is a constant equals to 4 for regime I and III and 2 for regime II, b_0 is the molecular thickness (ca. 5.71 Å for PTT [31]), σ is the lateral-surface free energy, and κ is Boltzmann constant. Here, it should be mentioned that Huang and Chang [9] directly used the b parameter of crystal unit cell as the molecular layer b_0 thickness for the chain folding of nucleation in PTT. This operation should be reconsidered because Suzie et al. [32] have suggested that the chain folding for nucleation takes place along the (010) crystal plane for PTT, and the b_0 value has been taken as the perpendicular separation of growth crystal plane [33]. The d-spacing ($d_{010} = b_0 = 5.71$ Å) between (010) crystal planes is not equal to the b parameter of crystal unit cell ($b = 6.26$ Å) because of the triclinic crystal for the unit cell of PTT. Generally, it is convenient to rewrite Eq. (3) as a logarithmic form as follows:

$$\log G + \left[\frac{-U^*}{2.303R(T_c - T_\infty)}\right] = \log G_0 - \frac{K_g}{2.303T_c(\Delta T)f} \quad (5)$$

For most polymers, the value of U^* is ca. 1500 cal mol^{-1} where $T_\infty = T_g - 30$ K is often used. In fact, it is difficult to estimate experimentally a correct U^* value. However, the U^* value will significantly affect the application of the theory in qualitative and quantitative estimations because a modification of this parameter would lead to a change in apparent regimes [12]. In the present work, we try to simulate the crystallization data for determining an appropriate U^* value through a common method reported in the literatures [12–15]. The simulation results from Eq. (5) using various assumed U^* values were shown in Fig. 4. At the lower T_c, the data diverge upwards and downwards with changing U^* value. Meanwhile, the U^* value of 2500 cal mol^{-1} could be determined to permit the best linear fit of the data, indicating that this value is relatively suitable for use in PTT. In the present work, the U^* value of 2500 cal mol^{-1} was used to analysis the full set of data through the secondary nucleation theory and the result is shown in Fig. 5. It clearly exhibits classical regime I → II and regime II → III transitions at 488 and 468 K, respectively. The K_{gI}/K_{gII} and K_{gIII}/K_{gII} values in PTT are ca. 2.1 and 2.4, respectively, which are close to theoretical prediction of $K_{gI} = K_{gII} = 2K_{gII}$. The calculated K_g values are listed in Table 2.

On the other hand, the lateral surface free energy, σ was commonly dealt with an empirical relationship as shown in Eq. (6) suggested by Lauritzen and Hoffman [15], which was based on an earlier empirical treatment proposed by Thomas and Stavely [34]

$$\sigma = \alpha(\Delta H_f)(a_0 b_0)^{1/2} \quad (6)$$

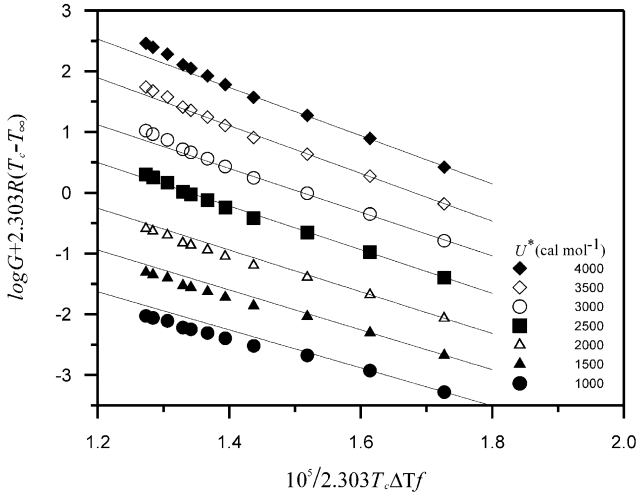

Fig. 4. Kinetic analysis of the growth rate data for PTT using several assumed values of U^*.

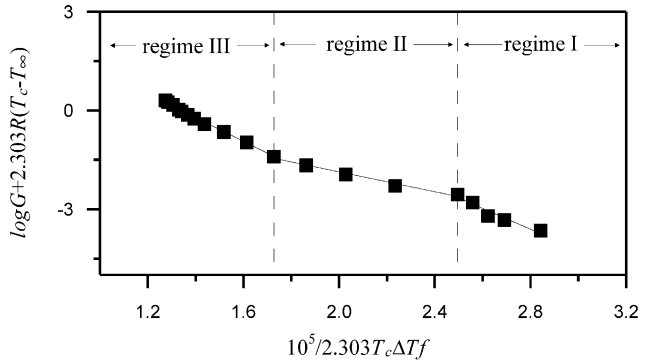

Fig. 5. Kinetic analysis of the full growth rate data using optimal values of $U^* = 2500$ cal mol^{-1}, and $T_\infty = T_g - 30$ K $= 288$ K.

The a_0 and b_0 factors are the molecular width and molecular layer thickness, respectively. Generally, the Thomas–Stavely constant, α, ranges between 0.1 and 0.3. The value of $\alpha = 0.1$ is widely applied in polyethylene [15] and other flexible polymers [35]. Roitman [33] and Marad [36] found that the α value was ca. 0.25 for polypivalolactone. The α value is not at all universal and strongly dependent on the chemical structure of polymer, and it is considered related to entropy differences between the crystal and melt interface [36]. How to determine the α value for PTT is an another operational problem, which affects significantly the quantitative estimation in the σ, σ_e and q values, because the work of chain folding for nucleation q is just defined as $2a_0b_0\sigma_e$ where the end surface free energy σ_e is commonly obtained from the $\sigma_e\sigma$ value by the application of Eqs. (4) and (6). Fortunately, Hoffman [37–39] has provided a relationship between the σ value and the characteristic ratio C_∞ as shown in Eq. (7)

$$\sigma = \Delta H_f(a_0/2)(1/C_\infty) \tag{7}$$

where a_0 is the molecular width (4.637 Å for PTT) [32], C_∞ is the characteristic ratio describing the unperturbed dimension of a polymer chain. The C_∞ value is generally defined as [40]

$$C_\infty = \frac{\langle r^2\rangle_0}{n_z l^2} \tag{8}$$

where n_z is the z-number of skeletal bonds along the chain, l is the average characteristic length over the number of bonds and $\langle r^2\rangle_0$ is the mean-square end-to-end distance of a long polymer chain in the unperturbed state. In order to conveniently estimate the $\langle r^2\rangle_0$ value, the Benoit's equation for peptidic chain [12,41] as given by Eq. (9) was used in this work where p designates the number of monomer units along the chain

$$\begin{aligned}\langle r^2\rangle_0 = {} & \frac{p}{1-\alpha\beta\gamma}\{(a^2+b^2+c^2)+2(ab\alpha+bc\beta+ca\gamma)\\ & +2ab\beta\gamma+bc\gamma\alpha+2ca\alpha\beta\}\\ & +2\frac{\alpha\beta\gamma^P-1}{1-\alpha\beta\gamma}\{\alpha\beta\gamma(ab\alpha+bc\beta+ac\alpha\beta)+ca\gamma\\ & +ab\beta\gamma+bc\alpha\gamma+(a^2+b^2+c^2)\alpha\beta\gamma\}\end{aligned} \tag{9}$$

The schematic diagram of Benoit's model to PTT, characteristic bond lengths (a, b and c) and supplementary angles (θ, φ and ϕ) involving main geometry are shown in Fig. 6. The C_∞ and $\langle r^2\rangle_0$ values obtained from Eqs. (8) and (9) are 2.14 and 30 259 Å, respectively. Through this procedure, the α and σ values could be easily obtained from Eqs. (6) and (7) by using the desired C_∞ value. From the definition of the K_g value in Eq. (4), one could obtain the $\sigma\sigma_e$ values for regime I, II and III. These calculated results are summarized and listed in Table 2. The α and σ values are 0.18 and 19.2 erg cm^{-2}, respectively. Both the α and C_∞ values in PTT are relatively smaller than those in PET ($\alpha = 0.20$ and $C_\infty = 2.48$) reported by Medellin-Rodriguez et al. [12], indicating that the chain flexibility of PTT is higher than that of PET. Incidentally, the α value for polyesters is very

Table 2
Kinetic data for crystallized PTT calculated from secondary nucleation theory ($T_\infty = T_g - 30$ K; $U^* = 2500$ cal/mol)

	Regime I	Regime II	Regime III
$K_g \times 10^5$ (K^2)	7.3	3.5	8.4
σ_e (erg/cm^2)	84.9	81.3	98.8
q (kcal/mol)	6.5	6.2	7.5
σ (erg/cm^2)		19.2	
K_{gI}/K_{gII}		2.1	
K_{gIII}/K_{gII}		2.4	

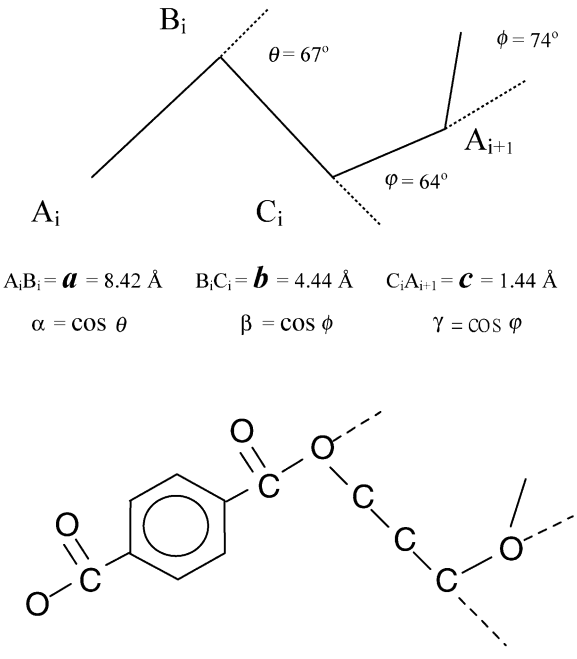

Fig. 6. Schematic diagram of Benoit's model representation of monomeric units with three virtual bonds for PTT.

different from that generally quoted for linear polyethylene ($\alpha = 0.10$). For less flexible polymers such as aromatic polyesters the α value should be larger than that for linear polyethylene with considering its physical meaning.

On the other hand, the work of chain folding q could be obtained directly from the fold-surface free energy, i.e. $q = 2\sigma_e a_0 b_0$. The q value is defined as the work for chain folding by bending the polymer chain back upon itself in the appropriate configuration that has been found to be a parameter most closely correlated with molecular structure, i.e. the inherent stiffness of the chain itself [15]. The q value of ca. 6–7 kcal mol^{-1} obtained in this work for PTT is relatively reasonable because it is smaller than that for PET (ca. 10 kcal mol^{-1}) [10] but larger than that for PBT (ca. 5 kcal mol^{-1}) [11]. It should be mentioned here that the q value of 4.8 kcal mol^{-1} for PTT reported by Huang and Chang [9] may be underestimated, because the α value of 0.1 was used for the calculation.

3.3. Temperature dependence of crystallization rate

When the crystallization takes place within a wide range of T_c, the temperature dependence of the Avrami rate constant k, i.e. the plot of k versus T_c should exhibit a typical bell-shaped curve. Therefore, the Arrhenius linear relation cannot be directly used to describe the temperature dependence of the rate constant k [42,43]. Generally, the k value is directly proportional to the rate of spherulite growth G, thus its temperature dependence could be described by the following equation:

$$k = k_0 \exp\left[\frac{-E_g}{R(T_c - T_g)}\right]\exp\left[\frac{-E_n}{R(T_m^0 - T_c)}\right] \quad (10)$$

The crystallization rate is controlled by the two well-established nucleation and diffusion mechanisms, which are characterized by opposite temperature dependences. Similarly, the temperature-dependence of overall activation energy can also be divided into two terms as shown in Eq. (10). The first term $E_g/(T_c - T_g)$ accounts for the temperature dependence of activation energy for diffusion process of the growing spherulites ($T_c - T_g$) being characteristic for mobility of the segments above T_g. The second term $E_n/(T_m^0 - T_c)$ is the temperature dependence of activation energy for nucleation process, ($T_m^0 - T_c$) being a measure of the undercooling of the melt. According to Eq. (10), the temperature dependence of the k value could be quantified by directly fitting the k values collected at various crystallization temperatures to one of the equations using the regression software. The corresponding fits for all of the Avrami rate constants are shown in Fig. 7. The unknown parameters such as E_g, E_n and k_0 provided by the software when the best fit was determined are taken to be 1650 cal mol^{-1}, 1480 cal mol^{-1} and 20 s^{-1}, respectively, and the correlation coefficient is 0.91. The dotted line in Fig. 9 represents the theoretical fits for the melt crystallization at $443 \leqq T_c \leqq 483$ K and the cold crystallization at

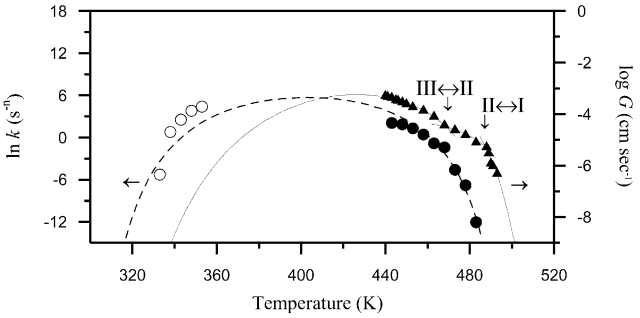

Fig. 7. Variation of ln k as a function of T_c. The dotted line and solid line represent theoretically predicted values from Eqs. (10) and (3), respectively. The experimental data of rate constant: (●) melt crystallization; (○) cold crystallization; (▲) linear spherulite growth.

$328 \leqq T_c \leqq 348$ K. The theoretical fitting curve of crystallization rate exhibits a bell-like shape, and the prediction of the maximum crystallization rate for PTT appears at ca. 410 K. The crystallization rate decreases significantly when T_c approaches either T_g or T_m^0. For cold crystallization, crystallization rate is considered to be dominated by the viscously driven diffusion process. The rate of cold crystallization was sharply increased with T_c. The aggregation rate of neighboring chains in cold crystallization was higher than that in melt crystallization at which the chain molecules reel in through reptation tube onto growth front.

On the other hand, the crystallization rate can be taken into account of secondary nucleation theory for melt crystallization. In this case, the G value is mainly governed by the rate of surface nucleation i and substrate completion rate g [37]. The experimentally determined growth rate versus temperature curve is also shown in Fig. 9 where the solid line is extrapolated from Eq. (3) using $U^* = 2500$ cal mol^{-1}, and the correlation coefficient is 0.97. The maximum crystallization rate appears at ca. 420 K. According to regime theory [37], growth rate curve exhibits breaks corresponding to regime I → II and regime II → III transitions. In regime I, the growth rate $G \propto i$ that one surface nucleus causes completion of a layer of length on the substrate. In the regime II, multiple surface nuclei begin to occur on the substrate because of the rapid increase of i associated with the larger undercooling and then $G \propto (ig)^{1/2}$. This leads to a downward break in the growth rate curve as one passes through the regime I → II transition when crystallization temperature is lowered. At further low temperature the mean niche separation characteristic of the substrate in regime II approaches the width of a stem, called regime III, in this regime $G \propto i$. Then, the regime II → III transition should cause an upswing break in the growth rate curve. For this reason, it may be thus considered that the regime I is diffusion-controlled process for $i/g \ll 1$, the regime II is diffusion and nucleation transition process for $i/g \sim 1$, and in regime III the growth rate is nucleation-controlled process for $i/g > 1$. In the present study the regime transition accompanied with morphological change of growing crystallite is discussed in detail in

Section 3.4. Incidentally, the crystallization rate curve in Fig. 7 is worthy of attention; the plot clearly indicates a discontinuity at $T_c = 468$ K for PTT. This result corresponds well with that stated in Fig. 5, i.e. the regime II → III transition temperature of 468 K for PTT. This transition temperature of PTT is higher than that of PET (438 K) [44] but lower than that of PBT (483 K) [11], implying that the regime behavior of nucleation may be mainly related to the chain flexibility.

3.4. Morphology of crystallite

Fig. 8 shows a series of PLM micrographs for PTT isothermally crystallized at various T_cs. In order to observe axialite-like crystallite formed at higher T_c, the micrograph of Fig. 8(l) was taken using an insertion of the $\lambda/4$ compensator. In all cases the nucleation density increases and spherulites texture becomes finer as T_c is decreased. The morphological change with T_c in PTT crystallite exhibits a normal trend, i.e. elliptical-shaped or axialite-like structure is formed at extremely high T_c and the spherulite is formed at relatively low T_c. When PTT was crystallized at $T_c =$ 493 K (Fig. 8(l)), the growing unit takes on an axialitic appearance and; it progressively changes into an elliptical-shaped structure (Fig. 8(k)) and then a spherulite-like structure (Fig. 8(j)) with decreasing T_c. Because the regime I → II transition occurs at 488 K, these crystallization temperatures are just located in the range of regime I. As T_c is further decreased (regime II), the banded spherulite is formed and the band spacing increases with increasing crystallization temperature beyond $T_c = 468$ K (Fig. 8(f)–(i)). At T_c below 468 K (regime II → III transition temperature), the banded structure disappears (Fig. 8(a)–(e)). This result in the formation of banded spherulite as PTT is in agreement with that reported by Ho et al. [7]. However, Wang et al. [8] reported that the banded spherulite of PTT could only be formed between 135 °C (408 K) and 165 °C (438 K) and the maximum growth temperature of spherulite is located at 165 °C. The temperature of $T_c = 165$ °C is also considered to be the upper limitation for PTT banded spherulite formation. In other words, the banded structure can only be formed in the lower half of the bell-shaped curve (log G versus T_c) down to the T_g. Because the very fast crystallization occurs at T_c close to the maximum growth temperature of spherulite ($T_c = 420$ K (147 °C) in this study), the PTT crystallization has already taken place during the quickly quenching process even at a cooling rate of ca. 100 K/min by PLM observation. The comparison with the result reported by Wang et al. is difficult to be made in the present study. Nevertheless, we do not favor that the formation of banded texture is directly related to the linear growth rate of spherulite. This is because the banded spherulite is also found at higher T_c (above 468 K) in this work and the band spacing increases with increasing T_c (form 9 μm at $T_c = 468$ K to 16 μm at $T_c = 483$ K) as shown in Fig. 8.

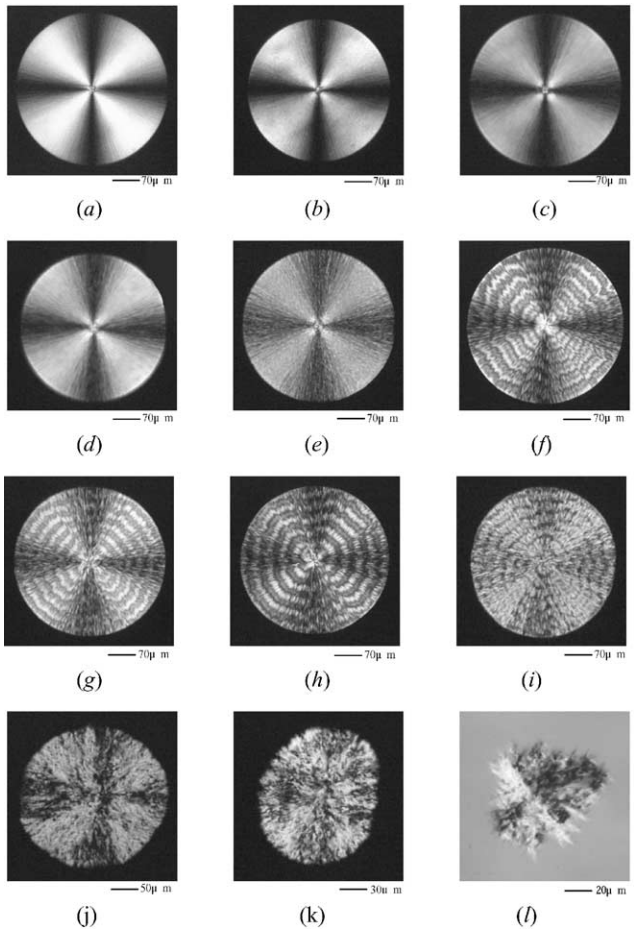

Fig. 8. PLM micrographs of PTT spherulites crystallized at (a) 443 K; (b) 448 K; (c) 453 K; (d) 458 K; (e) 463 K; (f) 468 K; (g) 473 K; (h) 478 K; (i) 483 K; (j) 488 K; (k) 490 K and (l) 493 K.

As stated above, the regime I → II → III transition of nucleation was accompanied by morphological changes from axialite-like or elliptical-shaped structures to banded spherulite and then non-banded spherulite. It should be mentioned here that the temperature limitation of banded spherulite formation is ca. 468 K at which the regime II → III transition occurs. This fact leads us to consider that the formation of banded spherulite in PTT may be related to the regime behavior of nucleation. Although, there are no other direct evidences to support whether this morphological change is really concerned with the regime behavior. It is well realized that the regime approach can be used to qualitatively discuss morphological changes of spherulite under various quenching depths. In regime II, the crystallization takes place at which nucleation and substrate completion rates are comparable. This condition is favor to make the lamellae to be well stacked for good spherulite growth. On the other hand, in regime III substrate completion is dominated by nucleation events and many nuclei would lead to disordered crystal growth. Under this condition, the disorganized lamellae are formed with many defects, resulting that good spherulite structure could not be produced. Since it is commonly believed that the periodic

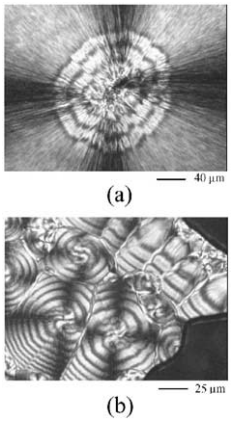

Fig. 9. (a) PLM micrograph of PTT spherulite successively crystallized under a series of T_cs (489 → 473 → 453 K, i.e. regime I → II → III). (b) PLM micrograph of PTT under non-isothermal crystallization.

extinction of banded spherulite is led by lamellar twist during growth [7], the well-stacked lamellae should be advantageous to form a periodic morphology for banded spherulite. In other words, the distorted lamellar structure formed in regime III and mostly immature and coarse spherulites formed in regime I are difficult to produce periodic twists for forming banded spherulite. Besides, the increase in band spacing with T_c may be related to larger thickness of lamellae formed at a rather higher T_c.

In order to confirm regime transition accompanied by a morphological change, Fig. 9(a) shows an example consisting of a variety of spherulite morphology at various T_cs from regime I to regime III where the successive growth of the spherulite is carried out. It is very clear that the center of spherulite shows an axialite-like structure in regime I (T_c = 489 K), and then banded spherulite is formed in regime II (T_c = 473 K). Finally, the non-banded spherulite is found in regime III (T_c = 453 K). This fact strongly suggests that the crystallization in regime II is indeed responsible for the formation of banded spherulite in PTT. Although, it is generally realized that the surface stress of the thin film induced by the deep quenching of melt sample would make the lamellae twist during crystallization for forming banded spherulite. Our result indicates that the banded morphology could also be formed in isothermal crystallization in order to compare the difference between these two banded spherulites formed from various crystallization mechanisms. Fig. 9(b) shows the spherulite structure of non-isothermally crystallized PTT, which the melt sample quickly quenched to room temperature. The banded spherulite having relatively regular concentric-circles was clearly found under this crystallization condition and the band spacing is much thinner (ca. 2 μm) than that of isothermally crystallized PTT in regime II. It is worth noting that the spherulites attached to edges of thin film also exhibit a banded texture. This fact directly indicates that the banded spherulites may be caused by deep quenching. The shrinking stress of film surface may lead to lamellar twist for forming banded structure. The formation mechanism of banded spherulite will be further discussed in detail in future.

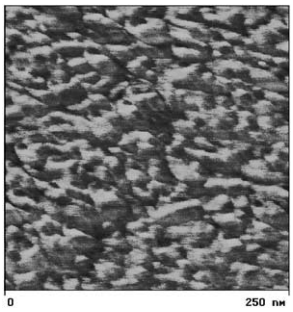

Fig. 10. AFM phase image of PTT from cold crystallization at T_c = 348 K.

The PTT spherulite exhibits a typical Maltese cross extinction and double concentric extinction rings in bended structure (Figs. 8 and 9), implying that the refractive indices vary periodically from $n_r > n_t$ through $n_r = n_t$ to $n_r < n_t$. The n_r and n_t are the refractive index in the direction parallel and perpendicular to the spherulite radius, respectively. For $n_r = n_t$ an optic axis is parallel to the incident beam, then the extinction takes place. According to the double extinction pattern of the spherulite and triclinic crystal for PTT, it is clear that there are two optic axes in the plane perpendicular to the spherulite radius. In addition, after insertion of the gypsum compensator, the interference color in the first and third quadrants of the cross is orange and in the second and fourth ones is blue, indicating that the negative spherulite is formed in PTT. Fig. 10 shows AFM photograph of PTT isothermally crystallized at T_c = 363 K (cold crystallization). The sheaf-like structure was found to be characterized by intermolecular aggregation in which a paracrystalline type order is present. This morphology corresponds well to the result in Avrami exponent of n = 5 for cold crystallization of PTT. The average size of sheaf-like structure is ca. 25 nm. The similar structure has been confirmed by the observation of transmission electron microscopy in cold crystallization of PET [45].

4. Conclusions

In this work, the isothermal crystallization kinetics of PTT was investigated from two crystallization temperature regions. PTT has been shown to follow an Avrami behavior in the primary stage of isothermal crystallization from the melt and glass states. The values of Avrami exponent were varied between 2 and 3 with crystallization temperature, indicating that the mixed growth and nucleation mechanisms may exist for melt crystallization. On the other hand, the Avrami exponent of n = 5 might correspond to a three-dimensional solid sheaf growth and athermal nucleation for cold crystallization. From the secondary nucleation analysis, one can estimate the free energies of the lateral

and folding surface, and the work of chain folding for nucleation. For aromatic polyesters, the crystallization rate and the work of chain folding for nucleation in increasing order is PBT > PTT > PET. Besides, a classical regime II → III transition of PTT was found at ca. 468 K that is higher than one of PET but lower than one of PBT. This is implied that the regime behavior of nucleation may be mainly related to the chain flexibility. The crystallite morphologies of PTT from melt and cold crystallizations exhibited typical negative spherulite and sheaf-like crystallite, respectively. The regime I → II → III transition was accompanied by morphological changes from axialite-like or elliptical-shaped crystallite to banded spherulite and then non-banded spherulite. In fact, it is still doubt whether the regime behavior of nucleation could dominate the formation of banded spherulite. Progress in understanding this phenomenon was much hindered by lack of detailed knowledge to elucidate their relation. Investigation of this phenomenon including both theory and experiment is required. It is unquestionable that the advance on this topic about the mechanism of band twisting is prerequisite.

References

[1] Brown HS, Chuah HH. Chem Fibers Int 1997;47(1):72.
[2] Chuah HH. Chem Fibers Int 1996;46(6):424.
[3] Dangayach K, Chuah HH, Gergen W, Dalton P, Smith F. Annu Tech Conf Soc Plast Engng 1997:2097.
[4] Ward IM, Wilding MA. J Polym Sci Polym Phys Ed 1976;14:263.
[5] Pyda M, Boller A, Grebowicz J, Chuah HH, Lebedev BV, Wunderlich B. J Polym Sci Part B: Polym Phys 1998;36:2499.
[6] Pyda M, Winderlich B. J Polym Sci Part B: Polym Phys 2000;38:622.
[7] Ho RM, Ke KZ, Chen M. Macromolecules 2000;33:7529.
[8] Wang B, Li CY, Hanzlicek J, Cheng SZD, Geil PH, Grebowicz J, Ho RM. Polymer 2001;42:7171.
[9] Huang JM, Chang FC. J Polym Sci Part B: Polym Phys 2000;38:934.
[10] van Antwerpen F, van Krevelen DW. J Polym Sci Polym Phys 1972;10:2423.
[11] Runt J, Miley DM, Zhang X, Gallagher KP, McFeaters K, Fishburn J. Macromolecules 1992;25:1929.
[12] Medellin-Rodriguez FJ, Phillips PJ, Lin JS. Macromolecules 1995;28:7744.
[13] Lovinger AJ, Davis DD, Padden Jr, F J. Polymer 1985;26:1595.
[14] Palys LH, Phillips PJ. J Polym Sci Polym Phys 1980;18:829.
[15] Hoffman JD, Davis GT, Lauritzen Jr. JI. In: Hannay NB, editor. Treatise on solid state chemistry, vol. 3. New York: Plenum Press, 1976. Chapter 7.
[16] Padden FJ, Keith HD. J Polym Sci 1959;39:101.
[17] Keith HD, Padden FJ. Polymer 1984;25:28.
[18] Keith HD, Padden FJ. Macromolecules 1996;29:7776.
[19] Keller A. J Polym Sci 1955;17:291.
[20] Chuah HH, Lin VD, Soni U. Polymer 2001;42:7137.
[21] Avrami M. J Chem Phys 1939;7:1103.
[22] Avrami M. J Chem Phys 1940;8:212.
[23] Avrami M. J Chem Phys 1941;9:177.
[24] Hillier IH. J Polym Sci (A) 1965;3:3067.
[25] Price FP. J Polym Sci (A) 1965;3:3079.
[26] Chuah HH. Polym Engng Sci 2001;41:308.
[27] Wunderlich B. Macromolecular physics, vol. 2. New York: Academic Press, 1976. Chapter 6.
[28] Jonsson H, Wallgren E, Hult A, Gedde UW. Macromolecules 1990;23:1041.
[29] Liu T, Mo Z, Wang S, Zhang H. Polym Engng Sci 1997;37:568.
[30] Chuang WT, Yeh WJ, Hong PD. J Appl Polym Sci 2002; 83:2426.
[31] Desborough IJ, Hall I, Neisser JZ. Polymer 1979;20:545.
[32] Suzie PD, Perez S, Revol JF, Brisse F. Polymer 1979;20:419.
[33] Roitman DB, Marand H, Miller RL, Hoffman JD. J Phys Chem 1989;93:6919.
[34] Thomas DG, Stavely LAK. J Chem Soc 1952:4569.
[35] Lauritzen Jr. JI, Hoffman JD. J Appl Phys 1973;4:4340.
[36] Marad H, Hoffman JD. Macromolecules 1990;23:3682.
[37] Hoffman JD. Polymer 1997;38:3151.
[38] Hoffman JD, Miller RL, Marand H, Roitman DB. Macromolecules 1992;25:2221.
[39] Hoffman JD. Polymer 1992;33:2643.
[40] Flory PJ. Statistical mechanics of chain molecules. New York: Oxford University Press, 1988.
[41] Benoit H. J Polym Sci 1948;3:376.
[42] Urbanovici E, Schneider HA, Cantow HJ. J Polym Sci Part B: Polym Phys 1997;35:359.
[43] Suupaphol P, Spruiell JE. Polymer 2001;40:699.
[44] Phillips PJ, Tseng HT. Macromolecules 1989;22:1649.
[45] Yeh GSY, Geil PH. J Macromol Sci B 1967;1:235.